Final Draft
of the original manuscript:

Epitaxial growth of nickel on Si(100) by dc magnetron sputtering

W. Kreuzpaintner,[a)] M. Störmer, D. Lott, D. Solina, and A. Schreyer
GKSS Forschungszentrum GmbH, Max-Planck-Straße 1, 21502 Geesthacht, Germany

The influence of the substrate temperature on the growth of highly textured Ni(111) and epitaxial Ni(200) with the relationships Ni[100]‖Si[110] and Ni(001)‖Si(001) on hydrogen terminated Si(100) wafer substrates by means of direct current magnetron sputtering is reported. In order to minimize crystal defect formation and to achieve a high quality epitaxial growth of Ni on Si, a two step deposition process was developed whereby different deposition conditions were used for an initial nickel seed layer and the remaining nickel film. The in-plane and out-of-plane structural properties of the films were investigated using x-ray scattering techniques, whereas magneto-optical Kerr effect and neutron reflectometry were used to confirm the magnetic nature of the epitaxially deposited nickel films. © *2008 American Institute of Physics*. [DOI: 10.1063/1.3032383]

I. INTRODUCTION

The growth of thin metallic films on silicon substrates has been widely studied owing to their importance in industrial applications,[1–7] including the ferromagnetic elements which are of particular interest for use in nonvolatile magnetic random access memory or spin-injection devices.[2,3,6,8] Silicon does not directly match the lattice constant of any of the ferromagnetic metals. Therefore, a copper seed layer is commonly employed when epitaxial growth is desired, known as metal-metal epitaxy on silicon (MMES). MMES has the advantage in that epitaxial growth at room temperature, without cooling or heating of the substrate, can be achieved for a variety of deposition methods, including molecular beam epitaxy and resistive heated or e-beam evaporation.[1,2,6,7,9–11] The disadvantage of MMES, however, is the potential contamination of the successive metallic layer by copper atoms during the deposition process or by interdiffusion.[12] Wet-chemical processes, e-beam evaporation, and ion-beam assisted deposition techniques have also been used to grow magnetic films of iron, cobalt, nickel, and their alloys directly on a single crystal silicon substrate, albeit with various results on the epitaxial quality.[11,13,14] A poor epitaxial crystal quality is particularly apparent for the case of nickel and publications of its epitaxial growth on silicon are rare.[13,15]

In general, it is assumed that epitaxial growth can only be achieved with low energy adsorbates and low deposition rates. Therefore, little attention has been given to the epitaxial growth of Ni on Si by means of magnetron sputtering, which is one of the most widely used thin film deposition techniques. It has been shown that copper can be deposited epitaxially on hydrogen terminated silicon surfaces by sputtering.[7] Both copper and nickel have a face-centered-cubic (fcc) structure and similar lattice constants. Therefore, it should be possible to grow epitaxial nickel on Si(100) by direct current (dc) magnetron sputtering. In this paper we show that this is in fact the case and demonstrate the feasibility of this technique for epitaxial growth of nickel on silicon with unprecedented quality.

II. EXPERIMENTAL PROCEDURE

A. Thin film preparation

A Si(100) wafer was cut to an appropriate substrate size of 20×60 mm^2 and ultrasonically cleaned using acetone followed by ethanol. Subsequently the native silicon oxide layer was removed using hydrofluoric acid, which also hydrogen terminated the silicon surface.[16,17]

Sputter deposition was carried out in a vacuum chamber with a base pressure of 1×10^{-8} mbar, equipped with two 7.62 cm dc magnetron sputter guns and a bakeable substrate holder. Indirect cooling of the substrate occurred by absorption of the blackbody radiation using a liquid nitrogen cryotrap, used to improve the vacuum quality. The distance between sputter target and substrate is approximately 25 cm at an angle of 22.5° to the substrate normal. Substrate temperature was monitored by a Pt/PtRh thermocouple and regulated within ±3 °C. Film thickness was time controlled using a shutter.

Only one sputter gun was equipped with a 99.99% pure nickel sputter target. Nickel was dc sputtered at 50 W with working gas of ultrahigh-purity argon at a pressure of 8.0×10^{-4} mbar resulting in a deposition rate of 0.2 Å/s. Prior to deposition, the substrate temperature was adjusted to the desired value and allowed to stabilize for approximately 2 h. The samples can be categorized by either continuous deposition with constant substrate temperature (type 1) or a two step deposition procedure whereby the substrate temperature is varied (type 2).

B. Film analysis

Out-of-plane structural analysis was made using a Bruker AXS D8 Advance two-circle x-ray diffractometer with parallel beam optics and Cu $K\alpha$ source. Conventional out-of-plane θ-θ diffraction scans were carried out to determine the crystalline structure, whereas "rocking" curves, also

---
a)Author to whom correspondence should be addressed. Electronic mail:
wolfgang.kreuzpaintner@gkss.de.

known as ω scans, are a measure of the mosaic spread or directional alignment of the crystallites. At a given film thickness, the full width at half maximum (FWHM) of the ω scans and both the FWHM and the peak intensities of the θ-θ scans are a measure of the epitaxial crystal quality. A lower FWHM value of the ω scans corresponds to a lower mosaic spread and hence a better directional alignment of crystallites and a better epitaxial quality. The size of the crystallites is analogous to the coherence length and can be determined by the Scherrer formula:[18]

$$B(2\theta) = \frac{0.94\lambda}{L\cos(\theta)}, \tag{1}$$

where $\lambda = 1.54$ Å, $B(2\theta)$ is the FWHM (in rad) of the powder diffraction peak, θ is the peak position (in rad), and L is the coherence length.

All samples were aligned with respect to the Si(400) out-of-plane substrate reflection, allowing for a well defined reference for the determination of any potential miscut of the silicon substrate and crystalline direction of the deposited nickel film. It should be noted that out-of-plane analysis is not sufficient for the examination of the epitaxial growth of a thin film as misalignment can occur in plane. Both out-of-plane and in-plane scans are needed to verify epitaxial growth (Figs. 3 and 6). A Seifert XRD 300 PTS four-circle x-ray diffractometer also utilizing Cu $K\alpha$ radiation with θ-2θ diffraction geometry and additional axes for sample inclination (χ) relative to the specular beam direction and axis rotation (ϕ) around the sample normal was used to access in-plane crystal information, allowing confirmation of uniform in-plane crystallite orientation. Alignment of the sample in ϕ and χ was made with reference to the Si(111) reflection. By setting the 2θ angle to the desired in-plane peak positions and rotating the sample around its normal ϕ at the corresponding inclination angle χ, information on the in-plane crystal symmetry can be obtained which also holds information on the epitaxial relationship of substrate crystal and deposited film. The instrument resolution of the x-ray diffractometers is defined by the FWHM of the Si(400) out-of-plane rocking curve and was smaller than 0.08°, which is small enough so that instrumental broadening in the analysis of the Ni films can be neglected.[19] X-ray reflectometry (XRR) was used to measure the thickness of the deposited layers.[20] Additionally, for type 2 samples magneto-optical Kerr effect (MOKE) and polarized neutron reflectometry (PNR) were used to probe the magnetization profile of the single layer and determine the magnetization of the thin film. MOKE uses the rotation of polarized laser light caused by the magnetic moments of the sample to probe the overall magnetic behavior, i.e., for measuring the magnetization of the sample in dependence on the applied magnetic field and its history. For PNR the value of the scattering amplitude of the polarized neutrons depends on the polarization state of the neutrons in respect to the magnetization of the sample. For the magnetic moments orientated collinear (+) or antiparallel ($-$) to the polarization vector of the neutrons, the total scattering length b_{tot} can be written as

$$b_{tot} = b_{nuclear} \pm p, \tag{2}$$

where $b_{nuclear}$ denotes the nuclear scattering length. The magnetic scattering length p can be calculated as

$$p = 0.27 \times 10^{-4} n\mu \frac{\lambda^2}{2\pi}, \tag{3}$$

where n is the density of the unit cell, λ is the applied wavelength, and μ is the magnetic moment in units of μ_B. The difference in the scattering amplitude leads to a shift in the reflectivity profiles which can be used to determine the magnetic part p and thus the magnetic moment of the layer. PNR was performed at the NERO neutron reflectometer at the Geesthacht Neutron Facility (GENF) of the GKSS Research Center which applies a neutron wavelength of 4.34 Å. Quantitative analysis of the XRR and PNR data was made using the PARRAT32 1.5.2 software package.[21]

III. RESULTS AND DISCUSSION

A. Type 1 samples

Out-of-plane x-ray diffraction (XRD) measurements in the range from 42° to 54° in 2θ of type 1 Ni films with film thickness of 75 nm are shown in Fig. 1 as a function of the substrate temperature. The observed intensities at $2\theta = 44.5°$ and at $2\theta = 51.8°$ correspond to the Ni(111) and Ni(200) reflections, respectively. At elevated temperatures ($T > 700$ °C) reflections at $2\theta = 42.4°$ and $2\theta = 53.4°$ can be observed. These correspond to (310) and (320) reflections of orthorhombic δ-Ni$_2$Si, indicating that at temperatures above 700 °C a Ni silicide phase is energetically favored over the growth of a separate Ni phase on Si(100).

Figure 1 clearly shows a maximum in the Ni(111) peak intensity with a corresponding minimum in the FWHM of the respective rocking curve at around 350 °C. Increasing substrate temperature causes the out-of-plane Ni(111) peak to disappear and the formation of a Ni(200) peak with maximum intensity and minimum FWHM rocking curve value at a substrate temperature of 625 °C. The intensities (Fig. 1) and coherence length of the Ni(200) reflections (Fig. 2) are significantly less compared to those observed for the Ni(111). Even if the expected intensity factor of the Ni(200) reflex of only 0.4 compared to that of the Ni(111) reflex is taken into account, these observations still clearly indicate that the out-of-plane texture of the Ni(200) is less pronounced than that of the Ni(111) directions.

Figure 3 gives the in-plane scan for the Si(111) substrate and the Ni(200) film peaks for the Ni(111) textured film deposited at 350 °C. The fourfold symmetry, typical for a cubic system, of the Si(111) reflections is clearly seen. However, no Ni(200) in-plane reflections were observed, showing that in-plane epitaxial growth of Ni(111) on Si(100) is not achievable as the grains are randomly oriented in plane.

In-plane ϕ scans of the type 1 sample with Ni(200) out-of-plane texture (substrate temperature: 650 °C) for Si(111) and Ni(111) reflections are shown in Fig. 4. In contrast to the Ni(111) textured films, a clear fourfold symmetry of the Ni(111) in-plane reflection is observed 45° to the Si(111) substrate peaks, demonstrating that nickel can grow epitaxi-

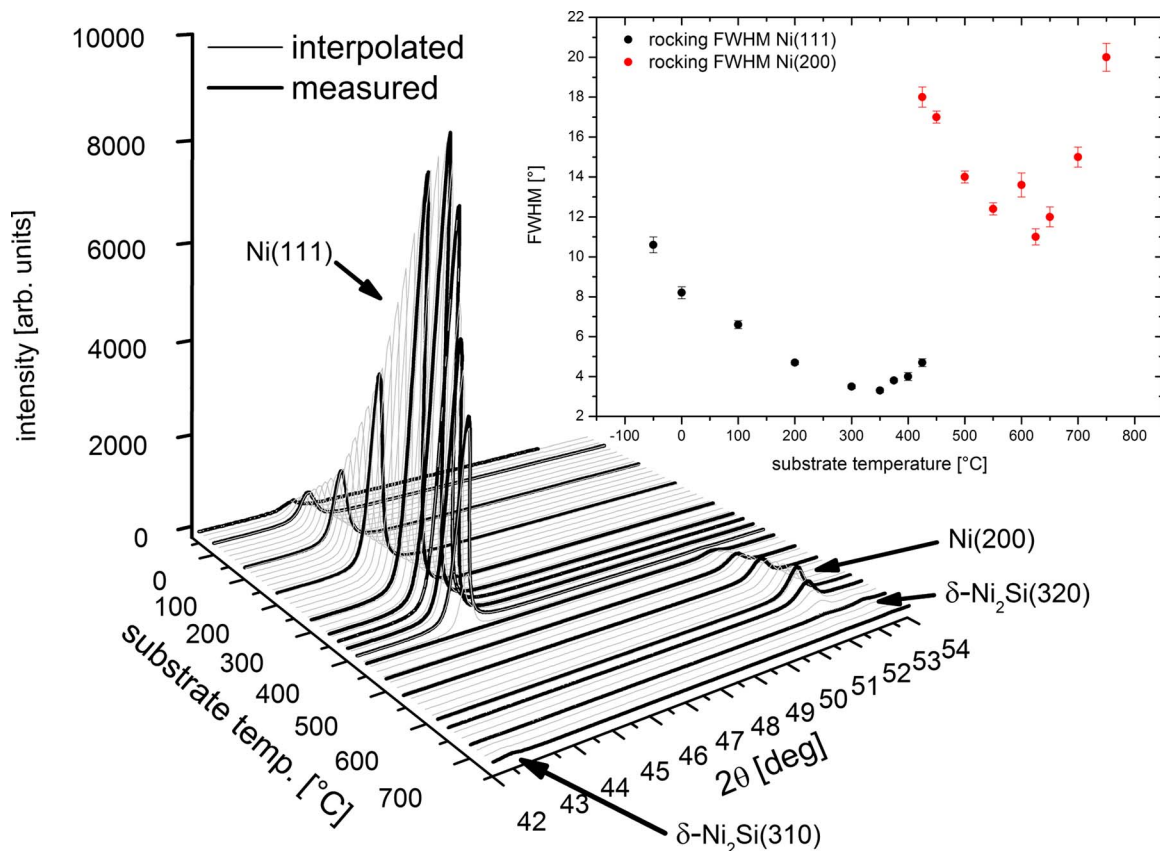FIG. 1. (Color online) The out-of-plane XRD scans from 42° to 54° in 2θ as a function of the substrate temperature during deposition. The inset graph gives the FWHM values of the corresponding out-of-plane rocking scans for Ni(111) and Ni(200).

ally on the Si(100) surface with the epitaxial relationships of Ni[100]‖Si[110] and Ni(001)‖Si(001). Even so, the observed Ni(111) reflections split into two, indicating the presence of twinning or the possible formation of small angle grain boundaries. The peak is split by $\Delta\phi=2.3°$ on either side of the expected Ni(111) peak position which is $\phi=45°$. The out-of-plane rocking scan for this sample is shown in the inset of Fig. 5, showing a splitting of $\Delta\omega=4.5°$ from the Ni[001] out-of-plane direction.

B. Type 2 samples

A significant increase in the quality of Ni(200) textured films could be obtained with a two step deposition process. The deposition parameters, the corresponding mosaic spread of the Ni(200) reflections, and the calculated coherence length are summarized in Table I. The coherence length for type 2 Ni(200) samples are greater than those of the type 1
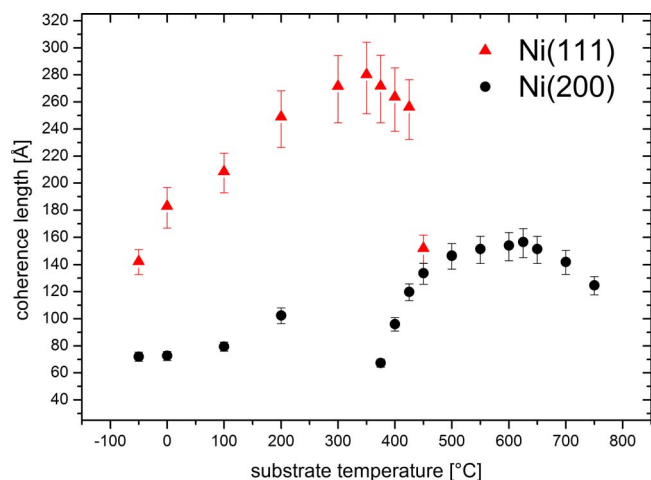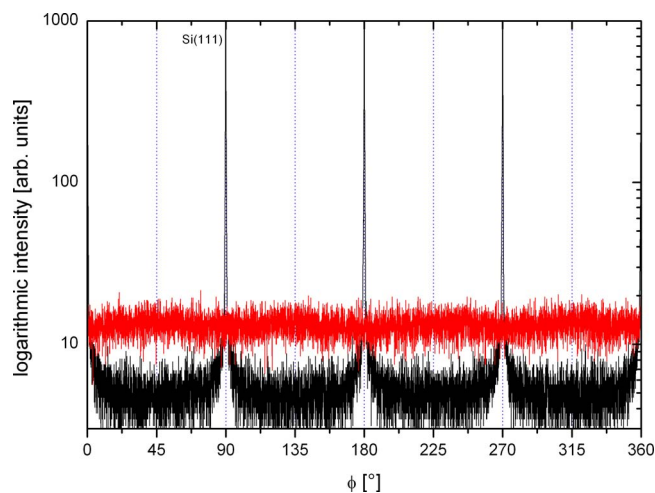

FIG. 2. (Color online) The coherence length values as a function of the substrate temperature during the deposition process as obtained from the out-of-plane XRD scans. The graph gives the coherence length values of both the Ni(111) and Ni(200) components.

FIG. 3. (Color online) The in-plane XRD scans for Si(111) and Ni(200) taken at 54.74° inclination to the (100) plane of the Si substrate. For growth parameters which favor a strong Ni(111) out-of-plane texture, no in-plane Ni(200) peak is visible, revealing that this direction does in fact not grow epitaxially on a Si(100) substrate.
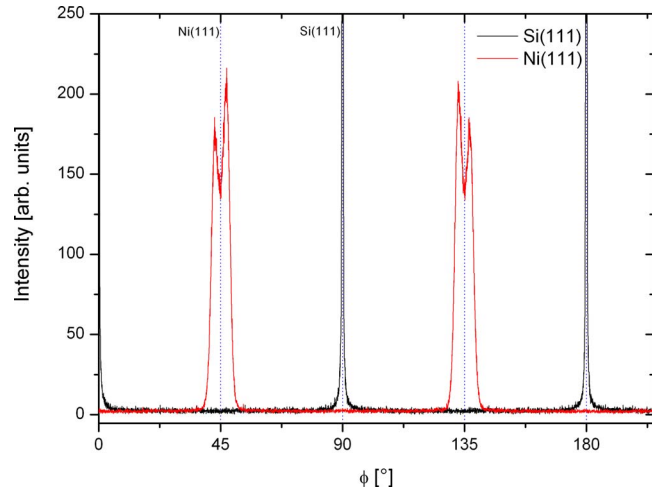
FIG. 4. (Color online) The in-plane scans with $\chi=54.74°$ for the Ni(111) and Si(111) for the sample which was deposited at 650 °C. For reasons of clarity, only a limited ϕ-range is shown.

Ni(200) samples, even though there is no clear tendency apparent to determine the ideal deposition parameters for epitaxial growth. The mosaic spread, however, gives a clear indication of the epitaxial growth. The XRD patterns for sample 2H (Table I) and the corresponding rocking scans are given in Fig. 5 and the in-plane Si(111) and Ni(111) reflections are given in Fig. 6.

The Ni(111) reflections show a fourfold symmetry with Ni(111) peaks at 45° to the Si(111) substrate peaks. Unlike type 1 samples, no splitting of the intensity is observed, indicating higher quality epitaxial growth.

Assessment of the interface quality was made with XRR and a simulated model is shown in Fig. 7. The model consists of three layers as indicated in the inset, i.e., Si/Ni/NiO$_x$/contamination. Attempts were also made to fit a four-layer model that included an additional silicide layer between the unoxidized nickel and the silicon in order to account for the two step deposition process of the nickel
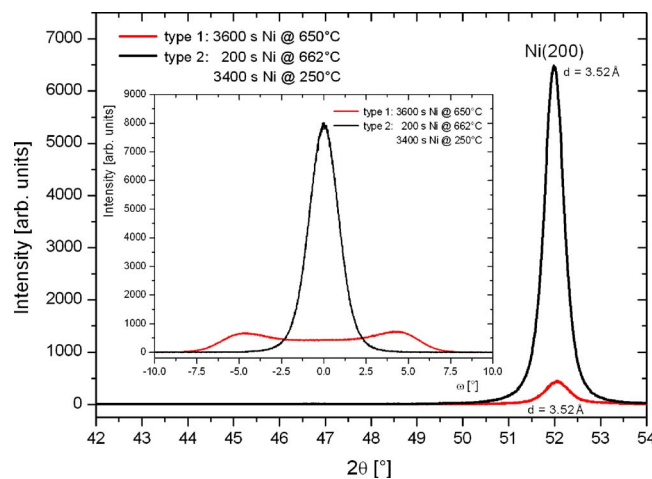
TABLE I. The out-of-plane FWHMs of the Ni(200) rocking scan peaks of 75 nm thick Ni with a total deposition time of 3600 s. Shown are also the temperatures (T_1, T_2) of the two deposition steps and the corresponding deposition times (t_1, t_2) as well as the coherence lengths (L) as obtained from the diffraction scans. The ideal deposition parameters for the lowest rocking FWHM found are underlined in the table.

Sample	T_1 (°C)	t_1 (s)	T_2 (°C)	t_2 (s)	$L_{Ni(200)}$ (Å)	FWHM$_{Ni(200)}$ (deg)
2A	550	200	325	3400	135	$16.4\ \binom{+0.6}{-0.6}$
2B	644	200	325	3400	181	$2.24\ \binom{+0.04}{-0.03}$
2C	662	200	325	3400	178	$2.20\ \binom{+0.05}{-0.03}$
2D	700	200	325	3400	188	$2.23\ \binom{+0.04}{-0.04}$
2E	750	200	325	3400	185	$2.24\ \binom{+0.04}{-0.05}$
2F	662	200	175	3400	181	$2.23\ \binom{+0.05}{-0.04}$
2G	662	200	212	3400	174	$2.23\ \binom{+0.04}{-0.04}$
2H	662	200	250	3400	185	$1.98\ \binom{+0.05}{-0.07}$
2I	662	200	287	3400	185	$2.16\ \binom{+0.04}{-0.04}$
2J	662	200	400	3400	196	$2.24\ \binom{+0.03}{-0.05}$
2K	662	100	250	3500	165	$2.80\ \binom{+0.06}{-0.05}$
2L	662	300	250	3300	178	$2.46\ \binom{+0.05}{-0.05}$
2M	662	400	250	3200	132	$7.3\ \binom{+0.3}{-0.2}$

film. However, the data were better fitted with the three-layer model, suggesting that the nickel layer grows as single layer on silicon.

Corresponding PNR data collected in a magnetic field of 80 mT at room temperature for the as-prepared Ni sample in a reciprocal space value range of $Q_z=0.01$ Å^{-1} to $Q_z=0.09$ Å^{-1} are shown in Fig. 8. This figure shows the neutron reflectivity data in dependence on the incoming polarization state of the neutrons with the corresponding MOKE measurement as the inset graph showing a squarelike behavior with sharp flipping fields symmetrically at about 20 mT. The remagnetization of the sample occurs completely at low magnetic fields in a single domain state. A clear shift in the curves is observed. By fitting the reflectivity using the standard PARRATT algorithm with $n_{Ni}=9.14\times10^{-2}$ Å^{-3} and $\lambda=4.34$ Å, the optimized value of the magnetic moment of the layer can be determined to be $\mu=0.6\mu_B$, which is identical to the bulk value of ferromagnetic Ni.[22] Moreover the

FIG. 5. (Color online) The out-of-plane XRD scan for the Ni(200) peak for the highest quality type 2 sample (with $d=3.52$ Å). For comparison the type 1 XRD scan of the sample which was deposited at a substrate temperature of 650 °C is shown, too ($d=3.52$ Å). The inset graph gives the corresponding out-of-plane rocking scans.
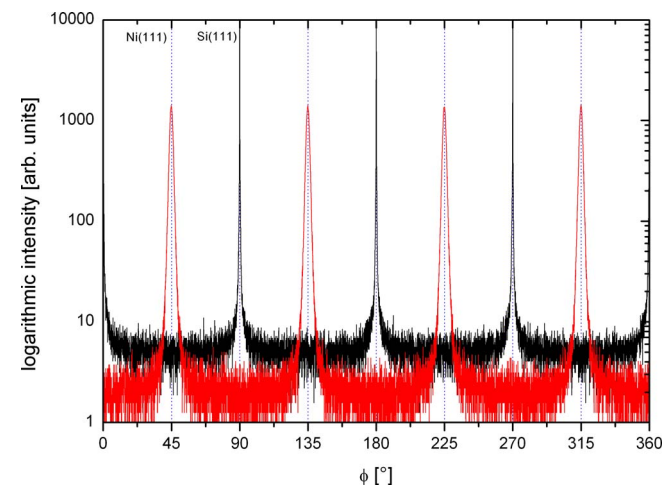

FIG. 6. (Color online) The in-plane XRD scans for Si(111) and Ni(111) taken at 54.74° inclination to the (100) plane of the Si substrate.
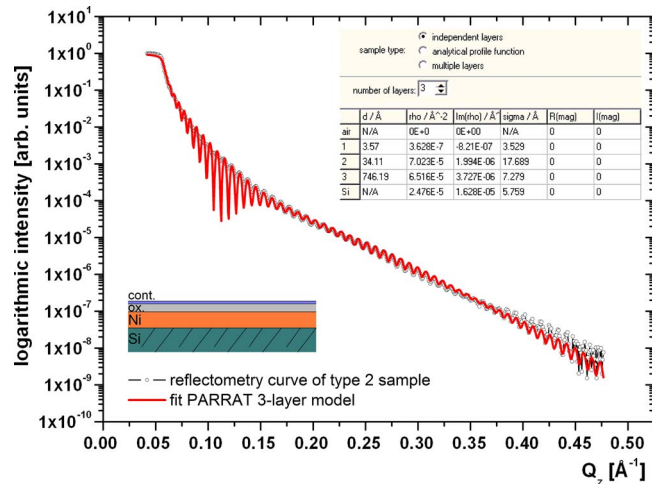
FIG. 7. (Color online) The XRR data of the type 2 sample with best epitaxial quality. A three-layer model was simulated. Starting from the surface, the first layer corresponds to an undefined contamination like condensed moisture from the air. The second layer can be interpreted as an oxidized Ni-to-air interface layer with the next layer being the unoxidized Ni layer which is in direct contact with the Si substrate.

reflectivity curves can be simulated best by assuming a homogeneous magnetization profile throughout the whole Ni layer and emphasize the excellent magnetic property of this epitaxial magnetic thin film of nickel on silicon. Hence, it is also concluded that the magnetic thickness of the nickel layer is identical to the structural thickness.

IV. DISCUSSION

A. Silicide formation

Potential formation of a silicide layer at the Si/Ni interface is an important issue and should be addressed. The literature shows for photoemission/Auger and ion scattering techniques[3,23,24] that nickel silicide formation takes place at the nickel to silicon substrate interface for temperatures above 200 °C that typically extends over approximately 10 ML. As the temperatures used in our work are well above the reported temperatures, silicide formation is expected, at least in the early stages of deposition; yet a silicide with a width
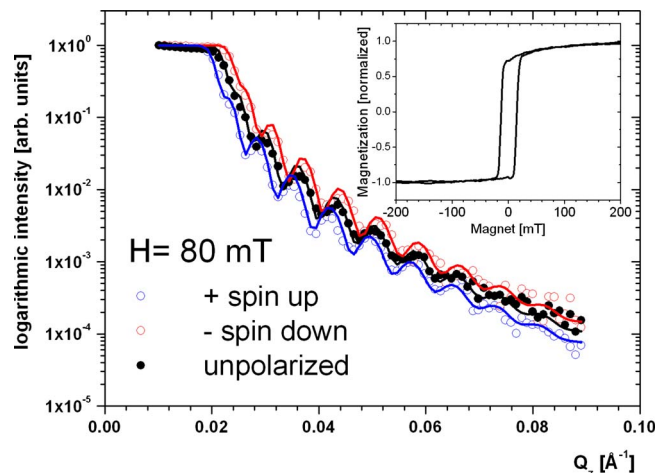

FIG. 8. (Color online) Unpolarized neutron reflectometry and PNR data points and fitted reflectivity curves (line) on sample 2H at a field of $H=80$ mT. The inset graph shows the corresponding MOKE measurement.

of only a few nanometers is too small to give sufficient phase diffraction for detection with conventional laboratory XRD methods. We observed no nickel silicide phases below a deposition temperature of 700 °C for type 1 samples and neither XRD nor XRR gave evidence of the presence of a silicide phase in the type 2 samples where an interface layer was assumed in an attempt to fit a four-layer model to the XRR data for the type 2 samples and gave a less perfect match (Fig. 7). The possible existence of an interface phase must be clarified by other methods such as systematic cross sectional transmission electron microscopy. As there was no epitaxial growth of Ni at temperatures when nickel silicide phases were present (>700 °C), it is concluded that nickel silicide negatively influences epitaxy and thus must be limited to a few atomic layers or would otherwise destroy epitaxial growth. As no silicide phase was observed with XRD below 700 °C, it will also be assumed that there is no nickel silicide phase present in our samples and subsequently assumed that nickel growth takes place directly on the silicon substrate without silicide formation.

B. Type 1 samples

There are a number of thermodynamic models for the growth of a thin layer on a substrate. Capillary theory[25,26] describes it by the preference for the Gibbs free enthalpy (G) to reach a minimum state with the free nucleation enthalpy given by

$$\Delta G = \Delta G_v a_1 r^3 + a_2 r^2 \gamma_{vl} + a_3 r^2 \gamma_{ls} + a_3 r^2 \gamma_{sv}, \quad (4)$$

where v stands for "vacuum," l for "layer," and s for "substrate." γ is the specific interface energy as derived from geometrical consideration. $a_1 = 2\frac{1}{3}\pi[2 - 3\cos(\theta) + \cos^3(\theta)]$, $a_2 = 2\pi[1 - \cos(\theta)]$, $a_3 = \pi\sin^2(\theta)$, and θ is the opening angle of the spherical sector of each layer seed. The Si surface is regarded as flat and the theory does not include any lattice match. Therefore, it cannot explain the observed epitaxial growth, but gives a satisfactory explanation for the observed polycrystalline and highly textured Ni(111) out-of-plane growth. For the epitaxial growth of Ni on Si, an epitaxial lattice rule match is employed based on the assumption that epitaxial growth takes place if substrate and film structure have a similar lattice constant with a misfit of typically less than 10%.

1. Textured growth of Ni(111)

The tendency to grow in a closest-packed direction is already well known for various metals.[27–29] At low substrate temperatures, one can assume that the adsorbates do not have sufficient energy to diffuse for large distances on the surface after their arrival at the substrate. In the capillary theory this case corresponds to the situation in which

$$\gamma_{sv} < \gamma_{ls} + \gamma_{vl}\cos(\theta), \quad (5)$$

which is the case if

$$\theta > 0.$$

Therefore adatoms form small nuclei whose diffusion on the surface is low; thus, in the first stages of the film growth

various crystal orientations occur and can persist. This sufficiently explains the observed film growth of our polycrystalline Ni films at low temperatures.

With increasing deposition temperature, the diffusion length of the adatoms also increases until a wetting of the entire surface takes place with the Young equation of the capillary theory being fulfilled,

$$\gamma_{sv} = \gamma_{ls} + \gamma_{vl} \cos(\theta), \tag{6}$$

which is the case if

$$\theta = 0.$$

This means that the previous Volmer–Weber (island) growth which was favored for lower deposition temperatures also changes to a Frank–van der Merve (layer-by-layer) growth. In fact, this naive point of view can be sufficient to explain the increasingly observed Ni(111) out-of-plane texture without a long-range epitaxial in-plane arrangement for the samples which were deposited at increasingly higher substrate temperatures. In this context the sample with the best observed Ni(111) texture would exactly correspond to the case in which perfect wetting of the Si substrate takes place.

Further increasing the substrate temperature means that the Young equation of the capillary theory can no longer be fulfilled, as the situation would become

$$\gamma_{sv} > \gamma_{ls} + \gamma_{vl} \cos(\theta). \tag{7}$$

Hence γ_{ls} and γ_{vl} would need to be density dependent or additional energy terms need to be introduced. In this situation Stranski–Krastanov (mixed-island and layer-by-layer) growth is expected to take place and can also be used for explaining the steep decrease in the Ni(111) texture after its maximum as was observed for our samples.

2. Growth of defect rich Ni(200) on Si(100)

With sufficient energy present in the system (i.e., high enough substrate temperature), one has to take the atomic structure of the substrate into account. In this scope, it would be very interesting to perform *ab initio* calculations in the style of Ref. 30, but would be beyond the scope of this paper. However, the phenomenological lattice match rule is sufficient to explain the results.

If one considers that Si has a diamond structure and Ni has a fcc structure, the uppermost unreconstructed atomic layer of the Si(100) plane surface has a quasi-two-dimensional rectangular structure with an expected bulk lattice spacing of 5.43 Å. Ni has a fcc structure and a bulk lattice constant of 3.52 Å. This results in a lattice mismatch of 54% along the {100} axes and hence is greater than the commonly accepted figure of approximately 10% as upper limit for lattice mismatch for epitaxial growth. The lattice mismatch decreases to 9% if Ni[100] arranges parallel to the Si[110] direction, which results in a 45° rotation around the [001] axis of silicon. This rotation was also observed experimentally by the in-plane XRD scans (Fig. 4) and therefore gives a satisfactory explanation for the epitaxial relationship as this relationship was also reported for sputter deposited copper.[7] The idealized situation on the Si/Ni interface is sketched in Fig. 9.
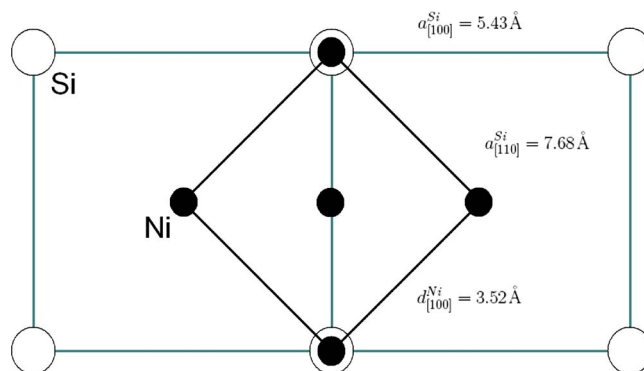

FIG. 9. (Color online) The epitaxial relationship of Ni to the Si(100) substrate. Shown are the last atomic layer of the Si substrate and the first atomic layer of the deposited Ni with their *d*-spacings of $d_{Ni(100)} = 3.52$ Å, $d_{Si(110)} = 7.68$ Å, and $d_{Si(100)} = 5.43$ Å. This relationship can directly explain the observed 45° rotation angle of the Ni layer crystal relative to the Si(100) substrate.

We show that the high temperatures of ≈ 650 °C are necessary and favor the initial stages of the just discussed epitaxial growth of Ni(200) on Si(100) where heteroepitaxy takes place. After the first few atomic nickel layers, the surface properties have significantly changed as the newly arriving nickel adatoms now grow on the already deposited nickel as their substrate. Consequently, the adjusted deposition parameters for the growth of nickel on silicon are not optimized for the autoepitaxial growth of nickel on nickel.

Assuming that (at a constant substrate temperature) with increasing nickel seed layer thickness the mobility of newly arriving adatoms also increases, then the occurrence of crystal defects can be explained: ideally, newly arriving atoms would diffuse on the surface until they reach a minimum energy state. At the highly elevated temperatures, present in our case, an atom might also simply fall into a state where its energy is only a local approximation to the global minimum. There it can act as a nucleation center for increasingly larger islands. It is known that with an increased mobility on the surface, adatoms have a tendency to form larger and less numerous nucleation centers than for the case where the adatoms have less surface mobility.[31]

These larger islands form at random locations owing to the nonminimized energy state. Consequently they do not all have the same lattice alignments and thus a misfit at the moment of coalescence must exist. If the islands were small they would rotate or change their positions on coalescence to accommodate for the misfits; however, larger islands are already too immobile to do this. Hence, crystal defects in the form of a small angle grain boundary related pattern can persist when the film growth takes place at too highly elevated temperatures as this crystal defect minimizes the energy of the overall system during growth.[25,32]

This can therefore sufficiently explain the structure of our type 1 samples with Ni(200) out-of-plane texture. The observed splitting in the rocking scan (inset of Fig. 5) of $\Delta\omega = 4.5°$ in either direction from the Ni[001] out-of-plane direction thus gives the out-of-plane angle between the reflecting planes and corresponds to an average lattice displacement of one extra or missing atom per ten atomic layers. At further increased temperatures the conditions are

favorable for silicide formation as evident from the disappearance of the Ni(200) phase and observation of the nickel silicide phases.

3. Type 2 samples

Based on the above explanations for the growth of nickel on Si(100) as a function of substrate temperature and therefore adatom diffusion mobility during deposition, one can also explain the observed enhanced epitaxial growth of out-of-plane Ni(200) on Si(100) if deposited in two steps. In stopping the growth process after the first initial high temperature step and giving the substrate sufficient time to cool down to more favorable temperatures for the epitaxial growth of nickel on nickel, one can remove the excess energy and therefore the too high adatom mobility from the system, which would otherwise cause crystal defects to form. This leads to the observed higher quality of epitaxial growth (Fig. 6). This technique of interrupted deposition is very similar to the MMES method, but instead of a copper seed layer, it uses the intended layer material (in our case nickel) for the deposition of the seed layer and would be best described as a single-element MMES. An insignificant disadvantage, however, is that the deposition cannot take place at room temperature.

The interrupted deposition of nickel on silicon also raises the question as to whether contamination takes place at the interface between the nickel seed and the successively deposited nickel. At the used deposition parameters (base pressure: 1×10^{-8} mbar; time between deposition steps: 2 h), this would be expected as the required time for the contamination of an atomically clean surface with one atomic layer of undefined residual gas adsorbates can be roughly estimated (by applying the kinetic gas theory and assuming a sticking coefficient of 1) by

$$Pt \approx 10^{-6} \text{ mbar s} = \text{const}, \tag{8}$$

where P is the pressure (in mbar) and t the time (in s).[33] This would mean that in the 2 h for which the deposition was interrupted between the Ni seed and the remaining nickel layer, an approximately 70 ML thick (and hence detectable) contamination layer of unknown composition would be expected; yet XRD and XRR show no evidence of a contamination. This may be a result of desorption processes that take place simultaneously. As desorption is strongly temperature dependent, the elevated temperatures of the substrate can significantly counteract the adsorption processes.[33] The situation on the Ni seed to nickel layer interface is currently only speculated and must still be investigated. It should also be noted that due to restrictions in the experimental setup (no active cooling of the substrate) the cooldown time could not be reduced. But it is expected that a shorter cooldown phase after the deposition of the initial seed layer would only decrease the likelihood of potential contamination and not destroy the observed epitaxial growth.

V. CONCLUSION

It was shown that it is possible to achieve epitaxial Ni(200) film growth directly on a Si(100) substrate by means of magnetron sputtering. The epitaxial relationship is Ni[100]∥Si[110] with Ni(001)∥Si(001) which was investigated by XRD techniques. Crystal defects in the Ni(200) layer growth were observed when using a one step deposition process, but could be prevented by interrupting the deposition process after an initial nickel seed layer. This delay does not influence the structural nor magnetic continuity of the nickel layer which was confirmed by XRD and XRR and PNR scans in conjunction with MOKE. Also, the advantage of a direct silicon to nickel interface and the fact that this deposition can be carried out by sputtering will certainly make this epitaxial Ni-layer-on-Si system interesting for applied research and hence may allow for the development of novel devices. Further investigations on the structural, magnetic, and electrical properties of the Ni(200)/Si(100) system are on the way and will be presented elsewhere.

[1] Y.-T. Cheng, Y.-L. Chen, M. M. Karmarkar, and W.-J. Meng, Appl. Phys. Lett. **59**, 953 (1991).
[2] C.-A. Chang, Appl. Phys. Lett. **58**, 1745 (1991).
[3] T. Nishimura, J. Takeda, Y. Asami, Y. Hoshino, and Y. Kido, Surf. Sci. **588**, 71 (2005).
[4] C.-A. Chang, J. C. Liu, and J. Angileilo, Appl. Phys. Lett. **57**, 2239 (1990).
[5] T. Ohmi, T. Saito, T. Shibata, and T. Nitta, Appl. Phys. Lett. **52**, 2236 (1988).
[6] G. Gubbiotti, G. Carlotti, C. Minarini, S. Loreti, R. Gunnella, and M. De Crescenzi, Surf. Sci. **449**, 218 (2000).
[7] H. Jiang, T. J. Klemmer, J. A. Barnard, and E. A. Payzant, J. Vac. Sci. Technol. A **16**, 3376 (1998).
[8] J. M. Daughton, Thin Solid Films **216**, 162 (1992).
[9] P. Castrucci, R. Gunnella, R. Bernardini, A. Montecchiari, R. Carboni, and M. De Crescenzi, Surf. Sci. **482–485**, 916 (2001).
[10] C.-A. Chang, J. Appl. Phys. **68**, 4873 (1990).
[11] C.-A. Chang, J. Magn. Magn. Mater. **109**, 43 (1992).
[12] A. M. Abdul-Lettif, Physica B **388**, 107 (2007).
[13] L. Wray and M. Prutton, Thin Solid Films **15**, 173 (1973).
[14] D. Berling, P. Bertoncini, A. Mehdaoui, P. Wetzel, G. Gewinner, and B. Loegel, J. Magn. Magn. Mater. **237**, 181 (2001).
[15] K. S. Grabowski, R. A. Kant, and S. B. Qadri, *Processing and Characterization of Materials Using Ion Beam*, MRS Symposia Proceedings, Vol. 128 (Materials Research Society, Pittsburgh, 1989), pp. 279–284.
[16] N. Hirashita, M. Kinoshita, I. Aikawa, and T. Ajioka, Appl. Phys. Lett. **56**, 451 (1990).
[17] V. A. Burrows, Y. J. Chabal, G. S. Higashi, K. Raghavachari, and S. B. Christman, Appl. Phys. Lett. **53**, 998 (1988).
[18] B. E. Warren, *X-ray Diffraction* (Dover, New York, 1990).
[19] B. D. Cullity, *Elements of X-ray Diffraction*, 2nd ed. (Addison-Wesley, Reading, MA, 1978).
[20] O. Durand, Thin Solid Films **450**, 51 (2004).
[21] BENSC HMI, "PARRATT32 or the Reflectivity Tool," http://www.hmi.de/bensc/instrumentation/instrumente/v6/refl/parratt_en.htm
[22] J. G. Louderback, A. J. Cox, L. J. Lising, D. C. Douglass, and L. A. Bloomfield, Z. Phys. D: At., Mol. Clusters **26**, 301 (1993).
[23] I. Abbati, L. Braicovich, B. De Michaelis, U. del Pennino, and S. Valeri, Solid State Commun. **43**, 199 (1982).
[24] G. L. P. Berning and L. L. Levenson, Thin Solid Films **55**, 473 (1978).
[25] K. L. Chopra, *Thin Film Phenomena* (McGraw-Hill, New York, 1969).
[26] T. Young, Philos. Trans. R. Soc. Lond. **95**, 65 (1805).
[27] M. Kawamura, Y. Abe, and K. Sasaki, Thin Solid Films **469–470**, 491 (2004).
[28] J. A. Thornton, Annu. Rev. Mater. Sci. **7**, 239 (1977).
[29] C. V. Thompson, Annu. Rev. Mater. Sci. **20**, 245 (1990).
[30] C. Ratsch, P. Ruggerone, and M. Scheffler, eprint arXiv:cond-mat/9709293v1 [cond-mat.mtrl-sci], 2008.
[31] K. L. Chopra and M. R. Randlett, Appl. Phys. Lett. **11**, 202 (1967).
[32] P. H. Leo and M. H. Schwartz, J. Mech. Phys. Solids **48**, 2539 (2000).
[33] M. Henzler and W. Gpel, *Oberflächenphysik des Festkörpers*, 2nd ed. (Teubner, Stuttgart, 1994) (in German).